Available online at www.sciencedirect.com
SCIENCE DIRECT®
Journal of Solid State Chemistry 178 (2005) 306–313
JOURNAL OF SOLID STATE CHEMISTRY
www.elsevier.com/locate/jssc

Hydrothermal synthesis, structural characterization and magnetic studies of the new pillared microporous ammonium Fe(III) carboxyethylphosphonate: $[NH_4][Fe_2(OH)\{O_3P(CH_2)_2CO_2\}_2]$

A. Anillo[a], A. Altomare[b], A.G.G. Moliterni[b], E.M. Bauer[c], C. Bellitto[c,*], M. Colapietro[d], G. Portalone[d], G. Righini[c]

[a]*Instituto de Química Organometálica "E. Moles", Departamento de Química Organica e Inorganica, Facultad de Quimica, c/Julian Claveria 8, Universidad de Oviedo, E-33006 Oviedo, Asturias, Spain*
[b]*Istituto di Cristallografia—CNR, Via Amendola 122, I-70125 Bari, Italy*
[c]*Istituto di Struttura della Materia—CNR, Sez. Montelibretti, Via Salaria km. 29.5, C.P. 10, I-00016 Monterotondo Staz., Roma, Italy*
[d]*Dipartimento di Chimica, Università di Roma "La Sapienza" P.le A. Moro, 00185 Roma, Italy*

Received 7 September 2004; received in revised form 28 October 2004; accepted 29 October 2004

Dedicated to Professor Julio Rodriguez, in memoriam

Abstract

The preparation by hydrothermal reaction and the crystal structure of the iron(III) carboxyethylphosphonate of formula $[NH_4][Fe_2(OH)\{O_3P(CH_2)_2CO_2\}_2]$ is reported. The green-yellow compound crystallizes in the monoclinic system, space group $Pc(n.7)$, with the following unit-cell parameters: $a = 7.193(3)$ Å, $b = 9.776(3)$ Å, $c = 10.17(4)$ Å and $\beta = 94.3(2)^\circ$. It shows a typical layered hybrid organic–inorganic structure featuring an alternation of organic and inorganic layers along the a-axis of the unit cell. The bifunctional ligand $[O_3P(CH_2)_2CO_2]^{3-}$ is deprotonated and acts as a linker between adjacent inorganic layers, to form pillars along the a-axis. The inorganic layers are made up of dinuclear Fe(III) units, formed by coordination of the metal ions with the oxygen atoms originating from the $[O_3P-]^{2-}$ end of the carboxyethylphosphonate molecules, the oxygen atoms of the $[-CO_2]^-$ end group of a ligand belonging to the adjacent layer and the oxygen atom of the bridged OH group. Each Fe(III) ion is six-coordinated in a very distorted octahedral environment. Within the dimer the Fe–Fe separation is found to be 3.5 Å, and the angle inside the [Fe(1)–O(11)–Fe(2)] dimers is ~124°. The resulting 3D framework contains micropores delimited by four adjacent dimers in the (bc) planes of the unit cell. These holes develop along the a-direction as tunnel-like pores and $[NH_4]^+$ cations are located there. The presence of the μ-hydroxo-bridged [Fe(1)–O(11)–Fe(2)] dimers in the lattice is also responsible for the magnetic behavior of the compound at low temperatures. The compound contains Fe^{3+} ions in the high-spin state and the two Fe(III) ions are antiferromagnetic coupled. The J/k value of −16.3 K is similar to those found for other μ-hydroxo-bridged Fe(III) dimeric systems having the same geometry.

Keywords: Ammonium Iron(III) carboxyethylphosphonate; Hydrothermal synthesis; X-ray crystal structure; Microporous pillared compound; Magnetic properties

1. Introduction

The phosphonate anion, $[RPO_3]^{2-}$, where R is an organic group, represents an interesting oxygen donor "building block" molecule. Its ability to give solid phases

*Corresponding author. Fax: +39 06 90672 316.
E-mail addresses: carlo.bellitto@ism.cnr.it (C. Bellitto), m.colapietro@caspur.it (M. Colapietro).

0022-4596/$ - see front matter © 2004 Elsevier Inc. All rights reserved.
doi:10.1016/j.jssc.2004.10.047

with a layered structure of the type M/O/P, when combined with divalent metal ions, M, renders this molecule suitable in the search for new inorganic–organic hybrid materials [1]. Moreover, in the case of paramagnetic metal(II) organophosphonates, the lamellar structure favors magnetic interactions between near-neighbors transition metal(II) ion centers and often a magnetic long-range ordering is established at low temperatures [2]. In addition, the molecular structure of the phosphonic acid can be chemically modified by connecting to the R group of the ligand another functional group, such as the $–NH_2$ group or the $–CO_2H$ or even another $–PO_3H_2$ group. These types of bifunctional ligands can then act as linkers and, according to the nature of the functional group that was used, a number of hybrids were designed, and recently a variety of compounds with layered and pillared structures have been isolated and characterized. Most of these studies have focused their attention on the chemistry of bifunctional metal(II) phosphonates, but only a few phosphonates containing transition metal(III) ions have been reported in literature until now [3–8]. The chemistry of transition metal(III) ions and bifunctional phosphonic acids of formula $R–(CH_2)_nPO_3H_2$, ($R = –NH_2$, $–CO_2H$), has been explored and the hydrothermal reaction between the $FeCl_3 \cdot nH_2O$ and the carboxyethylphosphonic anion ligand, i.e., $[O_3P(CH_2)_2CO_2]^{3-}$ has been studied. The hydrothermal reaction was carried out in the presence of urea in order to increase slowly the pH of the reaction mixture up to almost neutral values. In this range of pH, the carboxyethylphosphonic acid is expected to be deprotonated and therefore both the functional groups of the phosphonate ligand can act as an O-donor ligand to the metal ion.

In this paper, we report the preparation and structural elucidation, as well as the magnetic properties as a function of temperature down to 2 K of a new microporous and pillared ammonium Fe(III) carboxyethylphosphonate of formula $[NH_4][Fe_2(OH)\{O_3P(CH_2)_2CO_2\}_2]$.

2. Experimental section

2.1. Materials and methods

$FeCl_3 \cdot 6H_2O$ (Merck), carboxyethylphosphonic acid, $HO_2C(CH_2)_2PO_3H_2$ (Aldrich Chemical Co.), and urea (Acros) were of analytical grade and were used as received. HPLC water was used as solvent.

2.2. Synthesis of $(NH_4)[Fe_2(OH)\{O_3P–(CH_2)_2CO_2\}_2]$

The compound was prepared by hydrothermal reaction of a mixture of $FeCl_3 \cdot 6H_2O$ (0.50 g, 1.85 mmol), carboxyethylphosphonic acid (1.02 g, 6.62 mmol), urea (0.46 g, 7.66 mmol) and deionized water, 8 mL. The molar ratios in the initial mixture were Fe:acid: urea:water = 1:3.6:4.14:240. Urea was added with the purpose of increasing the pH of the solution. The carboxyethylphosphonic acid presents three different acidities: two from the phosphonic group and one from the carboxylic group, with respective pK_a values of 2.2, 4.6 and 7.7 [6a]. The mixture was placed in a small beaker (20 mL) and transferred inside a Teflon vessel containing water on the bottom. The vessel was then placed in a Parr digestion bomb and the latter closed up. The bomb was heated at 160 °C with a heating rate of $3° h^{-1}$ and left to react under autogenous pressure for 3 days. The bomb was cooled down to room temperature. The resulting product consisted of two phases: i.e., a light orange powder as a suspension in water and a green-yellow microcrystalline powder on the bottom of the beaker. The final pH of the solution was 5.2. The light orange suspension was separated from the yellow crystalline powder by decantation. The green-yellow microcrystalline compound was filtrated, washed with water and dried under vacuum (yield 40%). Several attempts of growing single crystals were made and, at last, a suitable but twinned crystal was isolated, when cyclohexane was added to the initial mixture (few mL). Analyses: Calcd. for $(NH_4)[Fe_2(OH)\{O_3P(CH_2)_2CO_2\}_2]$, $C_6H_{13}NO_{11}P_2Fe_2$: C = 16.05%; H = 2.92%; N = 3.12%. Found: C = 16.01%; H = 2.96%; N = 3.09%.

2.3. Characterization and physical measurements

Elemental analyses were carried out by the Servizio di Microanalisi—Istituto Struttura della Materia C.N.R. and by the Laboratorio de Análisis Cuantitativo Elemental of the University of Oviedo (Spain). Thermogravimetric (TGA) data were obtained in flowing dry nitrogen at a heating rate of $10° min^{-1}$ on a Stanton-Redcroft STA-781 thermoanalyzer. The FT-IR absorption spectra were recorded on a Perkin Elmer 621 spectrophotometer using KBr pellets. Static magnetic susceptibility measurements were performed by using a Quantum Design MPMS5 SQUID magnetometer in fields up to 5 T. A cellulose capsule was filled with a freshly prepared polycrystalline sample and placed inside a polyethylene straw to the end of the sample rod. All the experimental data were corrected for the core magnetization using Pascal's constants.

2.4. X-ray powder data collection

Room-temperature X-ray powder diffraction data were recorded on a Seifert XRD-3000 diffractometer, Bragg-Brentano geometry, equipped with a curved graphite monochromator [$\lambda(CuK\alpha_1) = 1.54056$ Å] and

a scintillation detector. The data were collected with a step size of 0.02° $\Delta 2\theta$ and at a count time of 8 s per step over the range $4° < 2\theta < 80°$. The powder sample was mounted on a stainless-steel sample holder. The diffractometer zero point was determined from an external Si standard.

2.5. X-ray single crystal structure analysis

A nearly cubic green-yellow single crystal of the title compound of the dimensions of ca. $0.1 \times 0.08 \times 0.08\,mm^3$ was mounted inside a glass fiber and used for data collection. Diffraction data were collected on a Huber CS diffractometer [9], with graphite monochromatized Mo$K\alpha$ radiation ($\lambda = 0.71069$ Å), using θ–2θ scan mode. The crystal used for diffraction studies was twinned and gave sets of reflections corresponding to the individual twins. The unit cell and the orientation matrix were determined by selecting the most intensive reflections. Details of the crystal data, data collection, structure solution and refinement are reported in Table 1. The crystal obtained showed a slight decomposition during the data collection. The structure was solved by direct methods [10], and refined isotropically by full-matrix least-squares method. All the hydrogen atoms were geometrically located and introduced into the final full-matrix least-squares refinement in a riding model with the isotropic temperature factors arbitrarily fixed. All final calculations were performed by SHELXL-97 and ORTEP-3 programs [11]. The final residuals ($(I > 2\sigma(I))$ were $R_1 = 0.135$ and $wR_2 = 0.368$. These residual values are higher than usual mainly because the data set could not be completely detwinned and the intensities of some reflections are overstimated due to probable twinning [12].

Table 1
Crystallographic data for $(NH_4)[Fe_2(OH)\{O_3P\text{–}(CH_2)_2CO_2\}_2]$

Crystal data	
$C_6H_{13}Fe_2NO_{11}P_2$	Mo$K\alpha$ radiation
$M_r = 448.77$	$\lambda = 0.71069$ Å
Monoclinic	Cell parameters from 30 reflections
Pc	$\theta = 3$–15
$a = 7.193\ (3)$ Å	$\mu = 2.315\,mm^{-1}$
$b = 9.776\ (3)$ Å	$T = 298\ (2)$ K
$c = 10.17\ (4)$	Cubic
$\beta = 94.3\ (2)°$	Green-yellow
$V = 713\ (3)$ Å^{-3}	$0.10 \times 0.08 \times 0.08\,mm^3$
$Z = 2$	
$D_x = 2.067\,mg\,m^{-3}$	
Data collection	
Huber CS four circle diffractometer	$\theta_{max} = 25°$
θ–2θ scan	$h = 0 \rightarrow 8$
1541 measured reflections	$k = 0 \rightarrow 11$
849 independent reflections	$l = -12 \rightarrow 12$
844 reflections with $I > 2\sigma(I)$	Three standard reflections monitored every 97 reflections intensity decay: 4%
$R_{int} = 0.0967$	
Refinement	
Refinement on F^2	$(\Delta/\sigma)_{max} = 0.000$
$R[F^2 > 2\sigma(F^2)] = 0.1347$	$\Delta\rho_{max} = 5.091$ e Å^{-3}
$wR(F^2) = 0.3679$	$\Delta\rho_{min} = -2.569$ e Å^{-3}
$S = 1.833$	
89 parameters	Scattering factors from *Internat. Tables for Crystallography* Vol. C
H-atom parameters constrained	
$w = 1/[\sigma^2(F_o^2) + (0.2000P)^2 + 0.0000P]$ where $P = (F_o^2 + 2F_c^2)/3$	

3. Results and discussion

A new ionic and polymeric compound of formula $(NH_4)[Fe_2(OH)\{O_3P\text{-}(CH_2)_2CO_2\}_2]$ was prepared from the hydrothermal reaction of $FeCl_3 \cdot 6H_2O$ and carboxyethylphosphonic acid in the presence of urea. Under these conditions urea hydrolyses to give ammonium carbonate. The latter rises gradually the pH of the solution up to 5.20, generates NH_4^+ cations and facilitates the deprotonation of all the donor groups of the phosphonic acid. A comparison with the results reported by Ferey et al. [8] shows that the pH of the final solution is critical for the synthesis of the compound. $(NH_4)[Fe_2(OH)\{O_3P\text{-}(CH_2)_2CO_2\}_2]$ is obtained from a hydrothermal reaction only when the final solution features a higher pH value and closer to neutrality. It has been isolated as a green-yellow microcrystalline powder and characterized by several techniques (elemental analyses, TGA and DSC, X-ray powder diffraction techniques as well as the electronic and FT-IR absorption spectroscopy). The TGA of the title compound is reported in Fig. 1. An initial loss of ~1.2% is observed and can be ascribed to the presence of less than 1/2 molecule of water of crystallization per formula unit. The next mass loss (13.8%) starts at 280 °C and stops at ~370 °C corresponding to the loss of ammonia and of the hydroxyl group. The compound further decomposes in different steps, and the total loss of 24.21% is observed at ~600 °C, a temperature at which the decomposition of the ligand (calcd. 25.84%) and the formation of $FePO_4$ occurs.

3.1. Structural characterization of $[NH_4^+][Fe_2(OH)\{O_3P(CH_2)_2CO_2\}_2]$

Attempts of growing single crystals for X-ray investigations were made and only twinned crystals were isolated. Twinning is not rare in these type of materials [12]. The structural characterization of the compound was then carried out by the combination of

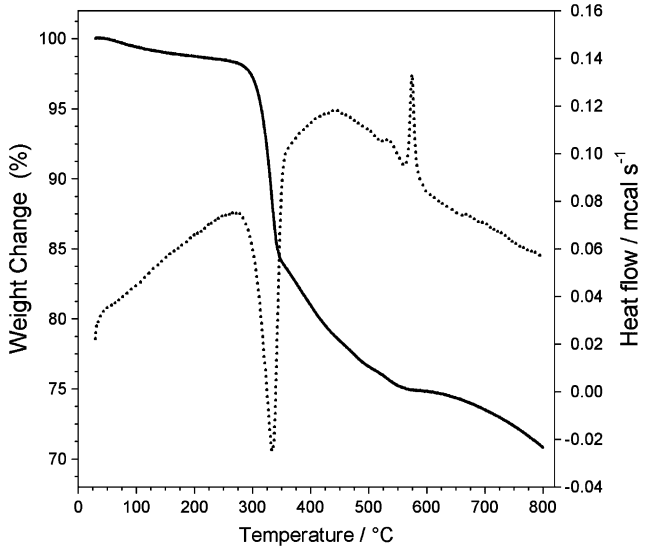

Fig. 1. TGA and DSC plots of $[NH_4][Fe_2(OH)\{O_3P(CH_2)_2CO_2\}_2]$.

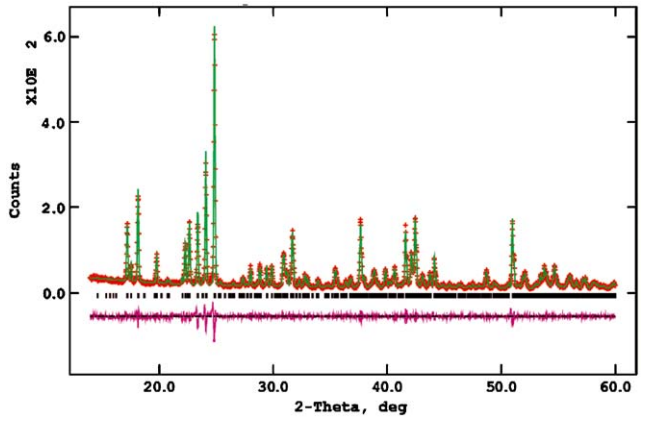

Fig. 2. Final observed (+ +), calculated (—) and difference plots for the Rietveld refinement against X-ray Powder diffraction patterns of $[NH_4][Fe_2(OH)\{O_3P(CH_2)_2CO_2\}_2]$.

the X-ray single crystal and X-ray powder diffraction techniques. These studies enabled us (a) to check the purity of the microcrystalline green-yellow powder from the other Fe(III) phase reported by Ferey [8a] and (b) to check the identity of the phase of the green-yellow microcrystalline powder and that one of the single crystal studied by X-ray single-crystal diffraction technique. The low-angle powder diffraction patterns of the title compound were indexed using the N-TREOR stand-alone program, [13a] suggesting a monoclinic unit cell with the following unit-cell parameters: $a = 7.178(1)$ Å, $b = 9.756(5)$ Å, $c = 10.128(5)$ Å and $\beta = 94.3(1)^\circ$. This indexing is characterized by the figure of merit $M'(20) = 69$ and $F(20) = 47$ (0.01014, 42). The X-ray powder diffraction pattern was refined by the Rietveld profile analysis [13b,c] using the model obtained by single-crystal studies and the results are reported in Fig. 2. These results clearly show that the green-yellow microcrystalline powder and the single crystal studied are the same compound. No extra peaks ascribed to the protonated $[Fe^{III}(OH)(H_2O)\{O_3P(CH_2)_2CO_2H\}]$ compound [8a] were found in experimental X-ray powder diffraction patterns.

3.2. Crystal and molecular structure description

The structure of the title compound consists of the polymeric $[Fe_2(OH)\{O_3P(CH_2)_2CO_2\}_2]^{-1}$ anions and ammonium ions. An ORTEP scheme of the asymmetric unit is shown in Fig. 3. The main bond distances and angles are reported in Table 2, other distances and angles may be found in the Supporting Information. The asymmetric unit consists of two iron atoms, one nitrogen atom, two completely deprotonated ligands and a μ-OH bridging group. In the resulting dimer, the Fe(1)–O(11) and Fe(2)–O(11) bonding distances are both equal to 2.01(3) Å. The angle Fe(1)–O(11)–Fe(2) is 124 (2)° and the Fe(1)–Fe(2) separation within the dimer is 3.54(2) Å. Both the Fe(III) sites are in a distorted octahedral symmetry and are coordinated by one oxygen from the bridged OH group and by three oxygens belonging to three different phosphonates in one side. The coordination around the metal ion is then completed by two oxygen atoms of the deprotonated carboxylate end of a neighboring ligand. Bond lengths around the Fe(1) ions range: Fe(1)–O(6)$[P(1)O_3^{2-}]$ = 2.00 (3) Å, Fe(1)–O(10)$[P(2)O_3^{2-}]$ = 1.93(3) Å, Fe(1)–O(5) $[(P(1)O_3^{2-}]$ = 1.99(3) Å and Fe(1)–O(1) $[C(1)O_2^{-1}]$ = 2.18(3) Å; Fe(1)–O(2) $[C(1)O_2^{-1}]$ = 2.09(3) Å, and Fe(1)–O(11) = 2.01(3) Å. The second octahedral chromophore $[Fe(2)O_6]$ of the dimer shows similar Fe–O bond

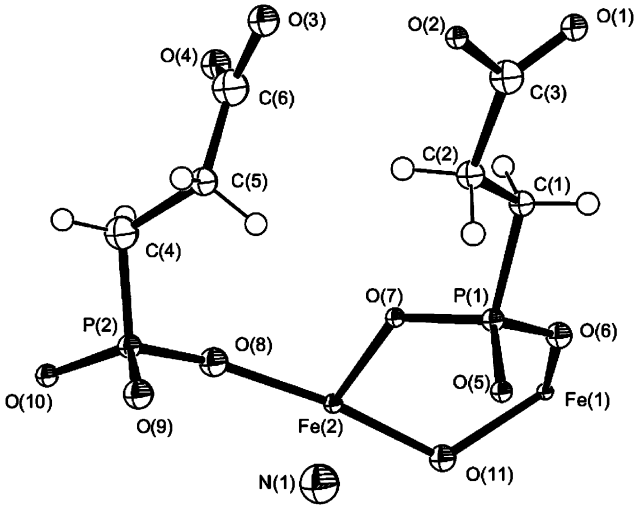

Fig. 3. Asymmetric unit of $[NH_4][Fe_2(OH)\{O_3P(CH_2)_2CO_2\}_2]$ showing the atom labeling. ORTEP drawing with 50% probability ellipsoids.

Table 2
Selected bond distances (Å) and angles (°) for $(NH_4)[Fe_2(OH)\{O_3P–(CH_2)_2CO_2\}_2]$.

Fe(1)–O(10)^{i}	1.93 (3)	P(1)–C(1)	1.82 (5)
Fe(1)–O(5)^{ii}	1.99 (3)	O(1)–C(3)	1.26 (6)
Fe(1)–O(6)	2.00 (3)	O(1)–Fe(1)^{v}	2.18 (3)
Fe(1)–O(11)	2.01 (3)	O(2)–C(3)	1.22 (5)
Fe(1)–O(2)^{iii}	2.09 (3)	O(2)–Fe(1)^{v}	2.09 (3)
Fe(1)–O(1)^{iii}	2.18 (3)	O(5)–Fe(1)^{vii}	1.99 (3)
P(1)–O(6)	1.48 (3)	O(10)–Fe(1)^{viii}	1.93 (3)
P(1)–O(5)	1.50 (3)	C(1)–C(2)	1.45 (6)
P(1)–O(7)	1.54 (3)	C(2)–C(3)	1.56 (6)
O(10)^{i}–Fe(1)–O(5)^{ii}	94 (1)	O(6)–P(1)–O(7)	112 (2)
O(10)^{i}–Fe(1)–O(6)	106 (1)	O(6)–P(1)–C(1)	104 (2)
O(10)^{i}–Fe(1)–O(2)^{iii}	157 (1)	O(5)–P(1)–O(7)	110 (2)
O(10)^{i}–Fe(1)–O(1)^{iii}	98 (1)	O(5)–P(1)–C(1)	109 (2)
O(10)^{i}–Fe(1)–O(11)	92 (1)	O(7)–P(1)–C(1)	108 (2)
O(5)^{ii}–Fe(1)–O(6)	90 (1)	P(1)–O(5)–Fe(1)^{vii}	143 (2)
O(5)^{ii}–Fe(1)–O(11)	173 (1)	P(1)–O(6)–Fe(1)	132 (2)
O(5)^{ii}–Fe(1)–O(2)^{iii}	84 (1)	P(1)–O(7)–Fe(2)	131 (2)
O(5)^{ii}–Fe(1)–O(1)^{iii}	84 (1)	P(2)–O(10)–Fe(1)^{viii}	138 (2)
O(6)–Fe(1)–O(11)	91 (1)	Fe(1)–O(11)–Fe(2)	124 (2)
O(6)–Fe(1)–O(2)^{iii}	97 (1)	C(2)–C(1)–P(1)	112 (3)
O(6)–Fe(1)–O(1)^{iii}	156 (1)	C(1)–C(2)–C(3)	118 (4)
O(11)–Fe(1)–O(2)^{iii}	91 (1)	O(2)–C(3)–O(1)	117 (4)
O(11)–Fe(1)–O(1)^{iii}	93 (1)	O(2)–C(3)–C(2)	120 (4)
O(2)^{iii}–Fe(1)–O(1)^{iii}	60 (1)	O(1)–C(3)–C(2)	122 (4)
O(6)–P(1)–O(5)	113 (1)		

Symmetry codes: (i) x, $-y$, $z-1/2$; (ii) x, $1-y$, $z-1/2$; (iii) $1+x$, $1-y$, $z-1/2$; (iv) $1+x$, y, z; (v) $x-1$; $1-y$, $1/2+z$; (vi) $x-1$, y, z; (vii) x, $1-y$, $1/2+z$; and (viii) x, $-y$, $1/2+z$.

distances and angles. All the Fe(III)–oxygen distances are in the range of the bond distances observed in previous reported Fe(III) phosphonates [6,8,14]. The μ(OH)-bridged Fe(III) dimers form a small cage, and each cage is bonded to adjacent ones by the third O(5) and O(8) atoms of the two different [–PO_3] groups, respectively. The inorganic layer is composed of these dinuclear units, the axes of which lie in the (*bc*) plane and are almost perpendicular to each other (see Fig. 5). The carboxyethylphosphonate ligand is bonded to the metal ions of two adjacent inorganic layers through both the ends of the organic moiety along the *a*-direction of the unit cell: one end of the ligand, i.e., the $[–CO_2]^-$ group, chelates to one Fe(III) ion C(3)–O(1) = 1.26(6) Å, C(3)–O(2) = 1.22(5) Å and the other end, i.e., the tetrahedral $[–PO_3]^{2-}$ group, binds the three oxygens to three different adjacent iron(III) ions lying in the adjacent inorganic layer (see Figs. 4 and 5). This pillared framework shows tunnel-like pores along the *a*-axis of the unit cell where $[NH_4]^+$ ions are located. It is interesting to point out that the size of the pore, estimated by taking into account the van der Waals radii of the oxygen atoms located inside the pore, is around 3.5 Å.

The electrostatic interactions, as well as hydrogen bonds involving the ammonium counter-ions, the coordinating carboxylate and phosphonate groups ensure the cohesion of the lattice.

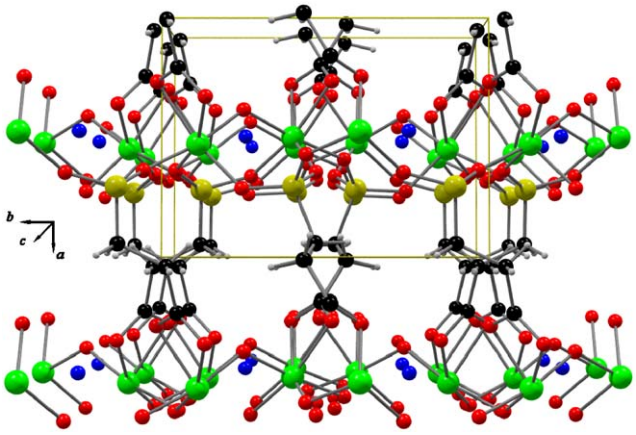

Fig. 4. A ball and stick representation of $[NH_4][Fe_2(OH)\{O_3P(CH_2)_2CO_2\}_2]$ viewed along the *c*-axis.

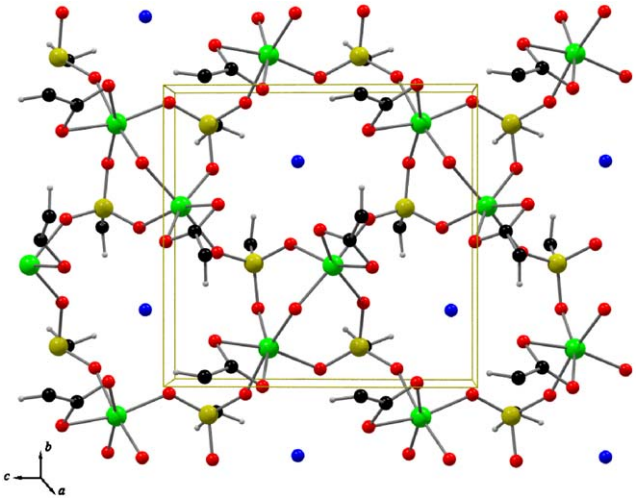

Fig. 5. A ball and stick representation of $[NH_4][Fe_2(OH)\{O_3P(CH_2)_2CO_2\}_2]$ viewed along the *a*-axis, showing the microporous structure.

3.3. Optical properties

IR spectroscopy provides a useful information on the molecular structure of the phosphonate ligands, in particular, on the protonation of their coordinating groups, such as the carboxylic and phosphonic groups. The FT-IR spectrum of $(NH_4)[Fe_2(OH)\{O_3P(CH_2)_2CO_2\}_2]$ is reported in Fig. 6. It features a sharp and intense band at 3622 cm^{-1} assignable to the –OH stretching vibration of the OH group. The sharp nature of this band indicates that the OH group is coordinated to the metal ions. The $N–H^+$ stretching vibrations of the $(NH_4)^+$ moiety are between 3280 and 3220 cm^{-1}, while the deformation should be located at ~1400 cm^{-1} [15]. The medium bands observed at 1530 and 1420 cm^{-1} are

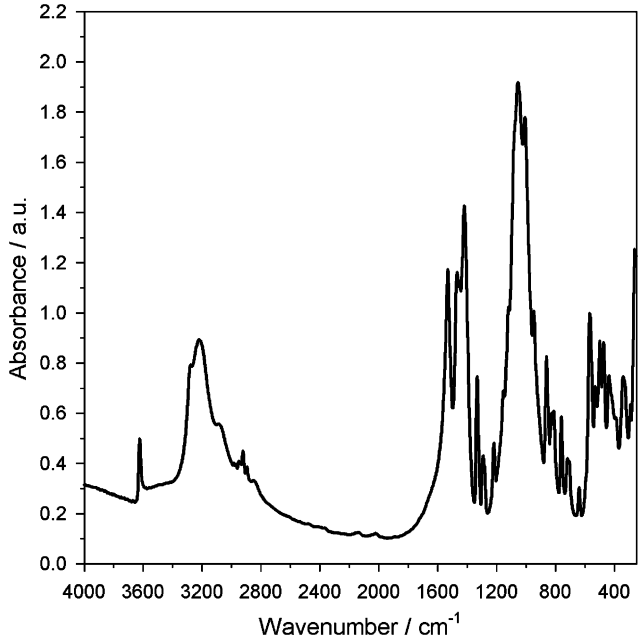

Fig. 6. FT-IR spectrum of $[NH_4][Fe_2(OH)\{O_3P(CH_2)_2CO_2\}_2]$ in the KBr region.

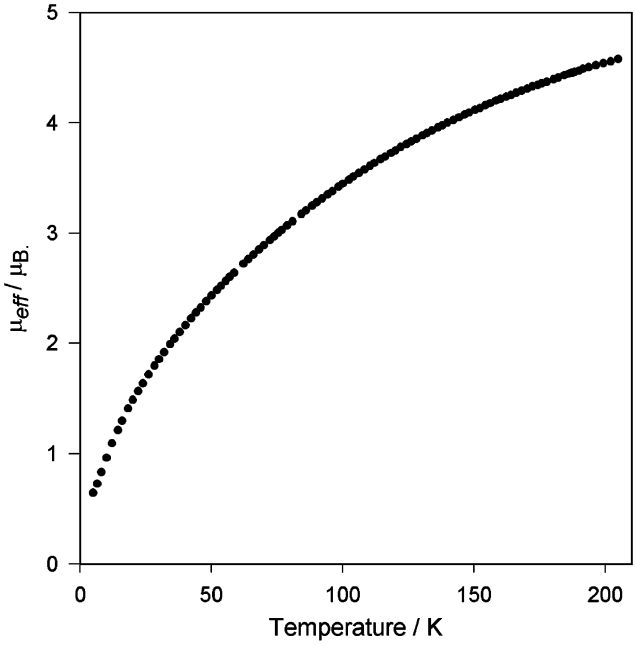

Fig. 7. Temperature dependence of the effective magnetic moment μ_{eff} per iron of the complex $[NH_4][Fe_2(OH)\{O_3P(CH_2)_2CO_2\}_2]$ in temperature region 5–200 K.

assigned to $\nu_{as}(CO_2^-)$ and to $\nu_s(CO_2^-)$, respectively, thus showing that also the carboxylic group is deprotonated [16] and in agreement with structural results. Three strong bands due to the $[PO_3]^{2-}$ group, i.e., symmetric (1010 and 944 cm^{-1}) and asymmetric (1054 cm^{-1}) vibrations, are observed in the range 1200–970 cm^{-1}. The complete conversion of the phosphonic acid group to its Fe(III) salt is demonstrated by the absence of OH stretching vibrations of the –POH group typically found at ~2700–2550 and 2350–2100 cm^{-1}. The symmetric and asymmetric (CH_2) stretches are located between 2900 and 2800 cm^{-1}.

The UV–visible reflectance spectrum has also been recorded and shows transitions at 380 nm(s), 439 nm(s), 584 nm(w), and 906 nm(w). The electronic behavior is confirmative of the presence of the Fe(III) ion (i.e., characterized by spin-forbidden bands and CT transition below 500 nm).

3.4. Magnetic properties

The magnetic properties of the title compound have been studied in the temperature range 250–2 K.

3.5. High-temperature region

The temperature dependence of the molar magnetic susceptibility, χ, of the title compound has been measured in the temperature range 5–250 K. The μ_{eff} vs. T plot is reported in Fig. 7. A deep decrease of the effective magnetic moment, μ_{eff}, on lowering the temperature is observed. The μ_{eff} value per dimer at 250 K is 7.04 μ_B, indicating the presence of high-spin Fe(III) species, [17] and falls to 0.7 μ_B at $T = 5$ K, thus suggesting antiferromagnetic intramolecular coupling. The plot χ_M vs. T, in the temperature range 5–200 K,

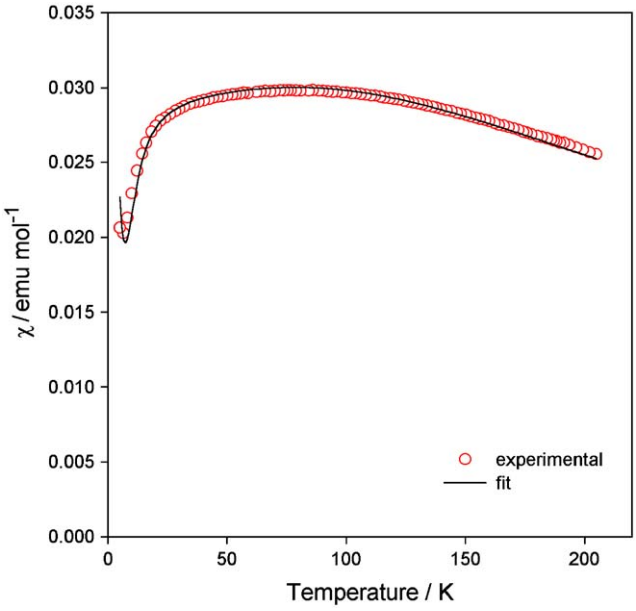

Fig. 8. Fit (solid line) and experimental (circles) χ_M vs. T plots of $(NH_4)[Fe_2(OH)\{O_3P(CH_2)_2CO_2\}_2]$ in the temperature region 5–200 K. The fit has been performed by using Eq. (1) and assuming a dinuclear molecular structure (see text).

shows a very broad maximum at $T\sim80$ K (see Fig. 8). This behavior is indicative of the presence of a μ-hydroxo bridged Fe(III) dinuclear structure in the system. Fig. 8 also reports the fit of the χ vs. T plot, which was performed by using the isotropic spin–spin interaction of the Heisenberg–Dirac–van Vleck Hamiltonian, $H=-2J\cdot S_1\cdot S_2$, where $S_1=S_2=5/2$ [18]. Solving the van Vleck equation for this Hamiltonian results in the following magnetic susceptibility equation (Eq. (1)) which was used to fit the experimental data:

$$\chi=(1-\chi_p)\frac{N_A\mu_B^2}{\kappa T}g^2 \times\left[\frac{2e^{2x}+10e^{6x}+28e^{12x}+60e^{20x}+110e^{30x}}{1+3e^{2x}+5e^{6x}+7e^{12x}+9e^{20x}+11e^{30x}}\right] +2x_p\frac{N_A\mu_B}{3\kappa T}g^2S(S+1)+2\mathrm{TIP} \quad (1)$$

with $x=J/k$T. J/k represents the intramolecular interaction between the Fe(III) centers within the dimer; N_A = Avogadro number; μ_B = Bohr magneton; χ_p = paramagnetic fraction of the monomeric Fe(III) impurities ($S=5/2$), g = spectroscopic splitting factor; k = Boltzmann factor, TIP is the temperature independent paramagnetism per monomers.

The best-fit parameters found were: $J/k=-16.3\pm0.1$ K, TIP $=2.5\times10^{-4}$ cm^3 mol^{-1} and $\chi_p=1.22\%$ The assumed g-value was 2.00, in accordance with a $^6A_{1g}$ ground state for the Fe(III) ion. The values of the coupling constant J/k are in the typical range of values found for μ-alkoxo or μ-hydroxo-bridged dinuclear Fe(III) systems [19,20].

3.6. Low-temperature region

The magnetic behavior of the compound down to $T=2$ K has also been studied (see Fig. S1) in order to check the existence of any long-range magnetic ordering. On cooling down from 10 to 3 K, χ_M decreases and a minimum is reached at $T\sim6$ K and then it increases again and this is ascribed to the presence of paramagnetic Fe^{3+} impurities. A complete overlap between the *zfc* and *fc* χ_M vs. T plots is observed and the hysteresis loop recorded at 3 K is found to be linear. These findings rule out the presence of a long-range magnetic ordering down to 2 K, as suggested also by the type of crystal and molecular structure.

4. Conclusions

The new organic–inorganic hybrid polymer of formula $[NH_4][Fe_2(OH)\{O_3P(CH_2)_2CO_2\}_2]$ has been prepared and structurally and magnetically characterized. Its crystal structure is layered and pillared, resulting in an alternation of organic and inorganic layers. The latter consists of dinuclear octahedral $[Fe_2(OH)O_{10}]$ units with Fe(III) ions bridged by a single μ-OH group. The bifunctional anionic ligand $[O_3P(CH_2)_2CO_2]^{3-}$ acts as a pillar along the *a*-direction of the unit cell, coordinating through the oxygen atoms of the donor groups to the metal ions and giving rise to the layered and porous network. Tunnel-like pores of $\sim$3.5 Å in size are present in the (*bc*) plane and they are delimited by four adjacent iron(III) dimers. They develop along the *a*-direction of the unit cell and contain the $[NH_4]^+$ cations. This feature might suggest the use of the compound as an ion-exchange material or catalyst. The magnetic and optical properties were correlated to the structure of the compound.

Acknowledgments

This work has been carried out in the framework of the bilateral Scientific Agreement between the CSIC (Spain) and the CNR (Italy). The Italian Ministry of the University and Research FIRB 2001 programme on "Ibridi organici inorganici funzionali" and European COST D14 program are acknowledged for the financial support. One of us (C.B.) thanks Dr. M. Green of the Royal Institution of Great Britain for performing magnetic susceptibility measurements below $T=4.2$ K.

Appendix A. Supplementary data

Crystallographic data (excluding structure factor) for the structure reported in this paper have been deposited with the Cambridge Crystallographic Data Center as supplementary publication no. CCDC 245647. Copies of the data can be obtained free of charge on application to CCDC, 12 Union Road, Cambridge CB2 1EZ, UK (fax: (44) 1223 336-033; e-mail: deposit@ccdc.cam.ac.uk).

The online version of this article contains additional supplementary data. Please visit doi:10.1016/j.jssc.2004.10.047.

References

[1] (a) A. Clearfield, Z. Wang, J. Chem. Soc., Dalton Trans. (2002) 2937–2947;
(b) A. Clearfield, Prog. Inorg. Chem. 47 (1998) 371–510;
(c) G. Alberti, in: J.M. Lehn (Ed.), Comprehensive Supramolecular Chemistry, vol. 7, Pergamon Press, Oxford, 1999, p. 151.
[2] (a) C. Bellitto, in: J.S. Miller, M. Drillon (Eds.), Magnetism: Molecules to Materials, vol. 2, Wiley-VCH, New York, 1998, pp. 425–456
(b) C. Mingotaud, P. Delhaes, M.W. Meisel, D.R. Talham, in: J.S. Miller, M. Drillon (Eds.), Magnetism, Molecules to Materials, vol. 2, Wiley-VCH, New York, 1998, pp. 457–484.
[3] (a) M. Casciola, U. Costantino, A. Peraio, T. Rega, Solid State Ionics 77 (1995) 229–233;

(b) F. Fredoueil, D. Massiot, D. Poojary, M. Bujoli-Doeuff, A. Clearfield, B. Bujoli, Chem. Commun. (1998) 175–176
(c) H.G. Harvey, B. Slater, M.P. Attfield, Chem. Eur. J. 10 (2004) 3270–3278.
[4] (a) M. Riou-Cavellec, M. Sanselme, N. Guillou, G. Ferey, Inorg. Chem. 40 (2001) 723–725;
(b) N. Stock, S.A. Frey, G.D. Stucky, A.K. Cheetham, J. Chem. Soc., Dalton Trans. (2000) 4292–4296;
(c) N. Stock, G.D. Stucky, A.K. Cheetham, Chem. Commun. (2000) 2277–2278;
(d) S. Ayyappan, G.N. Diaz de Delgado, G. Ferey, A.K. Cheetham, C.N.R. Rao, J. Chem. Soc. Dalton Trans. (1999) 2905–2907;
(e) P. Rabu, P. Janvier, B. Bujoli, J. Mater. Chem. 9 (1999) 1323–1326;
(f) A. Distler, S.C. Sevov, Chem. Commun. (1998) 959–960;
(g) X.-M. Zhang, Eur. J. Inorg. Chem. (2004) 544–548.
[5] (a) C. Bellitto, M. Colapietro, E.M. Bauer, G. Portalone, G. Righini, Inorg. Chem. 42 (2003) 6345–6351;
(b) N. Guillou, Q. Gao, M. Nogues, A.K. Cheetham, G. Ferey, Solid State Sci. 4 (2002) 1179–1185;
(c) A. Distler, D.L. Lohse, S.C. Sevov, J. Chem. Soc. Dalton Trans. (1999) 1805–1812;
(d) D.M. Poojary, B. Zhang, A. Clearfield, J. Am. Chem. Soc. 119 (1997) 12550–12555;
(e) N. Guillou, Q. Gao, M. Nogues, A.K. Cheetham, G. Ferey, Chem. Mater. 11 (1999) 2937–2947.
[6] (a) F. Serpaggi, G. Ferey, Inorg. Chem. 38 (1999) 4741–4744;
(b) A. Cabeza, M.G.A. Aranda, S. Bruque, D.M. Poojary, A. Clearfield, Mater. Res. Bull. 33 (1998) 1265–1274;
(c) B.C. Borja, J. Hernzag, M. dos Santos Alfonso, Polyhedron 20 (2001) 1821–1830.
[7] (a) M. Riou-Cavellec, M. Sanselme, M. Nogues, J.M. Greneche, G. Ferey, Solid State Sci. 4 (2002) 619–625;
(b) B. Bujoli, P. Palvadeau, J. Rouxel, Chem. Mater. 2 (1990) 582–589.
[8] (a) M. Riou-Cavellec, M. Sanselme, M. Nogues, J.M. Greneche, G. Ferey, Solid State Sci. 2 (2000) 717–724;
(b) M. Sanselme, M. Riou-Cavellec, J.M. Greneche, G. Ferey, J. Solid State Chem. 164 (2002) 354–360.
[9] M. Colapietro, G. Cappuccio, C. Marciante, A. Pifferi, R. Spagna, J.R. Helliwell, J. Appl. Crystallogr. 25 (1992) 192–194.
[10] A. Altomare, M.C. Burla, M. Camalli, G. Cascarano, C. Giacovazzo, A. Guagliardi, A.G.G. Moliterni, G. Polidori, R. Spagna, J. Appl. Crystallogr. 32 (1999) 115–119.
[11] (a) G.M. Sheldrick, SHELXTL—97, Program for the Refinement of Crystal Structures, University of Göttingen, Germany, 1997;
(b) L.J. Farrugia, J. Appl. Crystallogr. 30 (1997) 565.
[12] H.G. Harvey, S.J. Teat, M.P. Attfield, J. Mater. Chem. 10 (2000) 2632–2633.
[13] (a) A. Altomare, C. Giacovazzo, A. Guagliardi, A.A.G. Moliterni, A. Rizzi, P.E. Werner, J. Appl. Crystallogr. 33 (2000) 1180–1186
(b) A.C. Larson, R.B. Von Dreele, GSAS: Generalized Structure Analysis System: Report LAUR 86-748, Los Alamos National Laboratory, Los Alamos, NM, 1994;
(c) B.H. Toby, EXPGUI a graphical user interface for GSAS, J. Appl. Cristallogr. 34 (2001) 210–213.
[14] E.I. Tolis, M. Helliwell, S. Langley, J. Raftery, R.E.P. Winpenny, Angew. Chem. Int. Ed. 42 (2003) 3804–3808.
[15] (a) K. Nakamoto, In Infrared and Raman Spectra of Inorganic and Coordination Compounds, third ed., Wiley, New York, 1978;
(b) G. Socrates, Infrared and Raman Characteristic Group Frequencies, Wiley, Chichester, 2001.
[16] A. Cabeza, M.A.G. Aranda, S. Bruque, J. Mater. Chem. 8 (1998) 2479–2485.
[17] B.N. Figgis, M.A. Hitchman, Introduction to Ligand-Fields and its Applications, Wiley-VCH, NewYork, 2000, p. 239.
[18] J. O'Connor, Prog. Inorg. Chem. 29 (1982) 204–276.
[19] (a) M. Scarpellini, A. Neves, A.J. Bortoluzzi, I. Vencato, V. Drago, W.A. Ortiz, C. Zucco, J. Chem. Soc. Dalton Trans. (2001) 2616–2623 and reference therein
(b) E. Coronado, J.R. Galan-Mascaros, C.J. Gomez-Garcia, J. Chem. Soc. Dalton Trans. (2000) 205–210.
[20] (a) P.N. Turowski, W.H. Amstrong, S. Liu, S.N. Brown, S.L. Lippard, Inorg. Chem. 33 (1994) 636–645;
(b) B. Krebs, K. Scheper, B. Bremer, G. Henkek, E. Althaus, W. Muller-Warmouth, K. Griesar, W. Haase, Inorg. Chem. 33 (1994) 1907–1914;
(c) K.E. Kaufmann, C.V. Popescu, Y. Dong, J.D. Lipschomb, L. Que Jr., E. Munck, J. Am. Chem. Soc. 120 (1998) 8739–8746.